Supplementary File

Physical Origin of Planar Linear Dichroism in van der Waals Semiconductors Using Main Group Elements

Qiang GAO[1,2], Yali YU[1,3], Kaiyao XIN[1,3], Ziqi ZHOU[1], Hui-Xiong DENG[1,3], Lin LI[4,5], Xiaojie TANG[4], Congxin XIA[4], Duan-Yang LIU,[1] Jian-Bai XIA[1,3], Jun KANG[2]*, Zhongming WEI[1,3]*

[1]State Key Laboratory of Superlattices and Microstructures, Institute of Semiconductors, Chinese Academy of Sciences, Beijing 100083, China

[2]Beijing Computational Science Research Center, Beijing 100193, China

[3]Center of Materials Science and Optoelectronics Engineering, University of Chinese Academy of Sciences, Beijing 100049, China

[4]School of Physics, Henan Key Laboratory of Photovoltaic Materials, Henan Normal University, Xinxiang 453007, China

[5]School of Physics and Optoelectronic Engineering, Zhengzhou Key Laboratory of Low-dimensional Quantum Materials and Devices, Zhongyuan University of Technology, Zhengzhou 450007, China

*Corresponding author (email: zmwei@semi.ac.cn, jkang@csrc.ac.cn)

Table of contents

		O	S	Se	Te	N	P	As
		N/A	N/A	N/A	Tellurene P-3m1	N/A	Phosphorene Pmna	Arsenene Pmna
C	Graphene P6/mmm	N/A	N/A	N/A	N/A	C_2N P6/mmm C_3N_4 P-6m2	N/A	AsC C2/m
Si	Silicene P6/mmm	N/A	SiS Pma2	SiSe Pma2	SiTe Pma2	SiN C2/m	SiP C2/m	SiAs C2/m
Ge	Germanene P6/mmm	GeO Pbcm	GeS Pmn2_1	GeSe Pmn2_1	GeTe Pmn2_1	GeN C2/m	GeP C2/m	GeAs C2/m
Sn	Stanene P6/mmm	SnO Pbcm	SnS Pmn2_1	SnSe Pmn2_1	SnTe Pmn2_1	SnN C2/m	SnP C2/m	SnAs C2/m
Sb	Antimonene P6/mmm	Sb_2O_3 Pmmn	Sb_2S_3 P2_1/m	Sb_2Se_3 P2_1/m	Sb_2Te_3 P2_1/m	SbN Pmn2_1	SbP Pmn2_1	SbAs Pmn2_1
Bi	Bismuthene P-3m1	Bi_2O_3 P2_1/m	Bi_2S_3 P2_1/m	Bi_2Se_3 P2_1/m	Bi_2Te_3 P2_1/m	BiN Pmn2_1	BiP Pmn2_1	BiAs Pmn2_1
B	Borophene P6/mmm	B_2O_3 Pmc2_1	B_2S_3 P2_1/m	B_2Se_3 P2_1/m	B_2Te_3 P2_1/m	BN P-6m2	BP P-6m2	BAs P-6m2
Al	N/A	Al_2O_3 Pc	Al_2S_3 P1	Al_2Se_3 P1	Al_2Te_3 P1	AlN P-6m2	AlP P-6m2	AlAs P-6m2
Ga	N/A	Ga_2O_3 Pc	Ga_2S_3 P1	Ga_2Se_3 P1	Ga_2Te_3 P1	GaN P-6m2	GaP P-6m2	GaAs P-6m2
In	N/A	In_2O_3 Pmn2_1	In_2S_3 P1	In_2Se_3 P1	In_2Te_3 P1	InN P-6m2	InP P-6m2	InAs P-6m2

Figure S1. Space groups for all 75 2D materials. The space group of each 2D material is labeled with international notation and lies below each material.

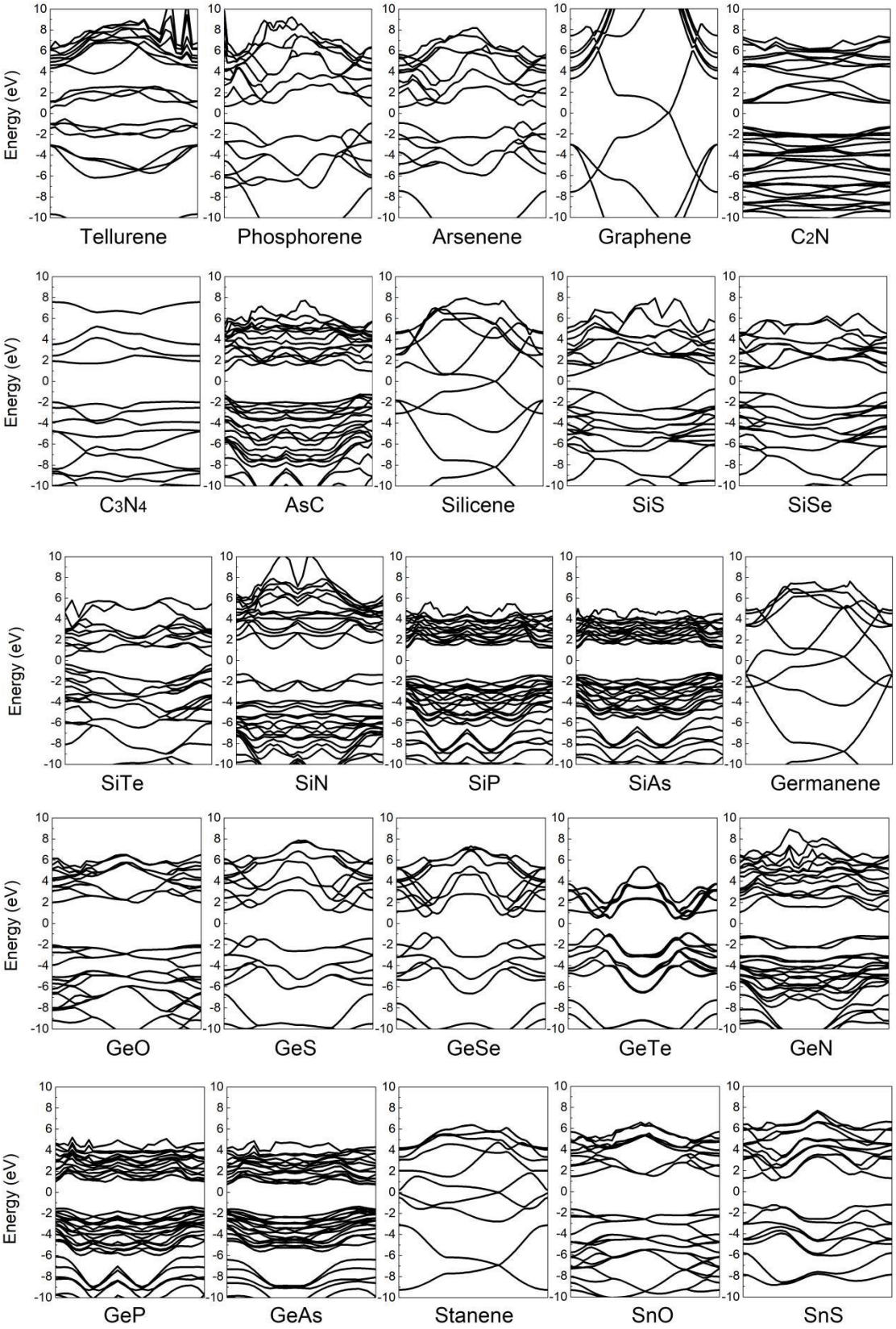
Energy (eV)
Tellurene
Phosphorene
Arsenene
Graphene
C2N
C3N4
AsC
Silicene
SiS
SiSe
SiTe
SiN
SiP
SiAs
Germanene
GeO
GeS
GeSe
GeTe
GeN
GeP
GeAs
Stanene
SnO
SnS

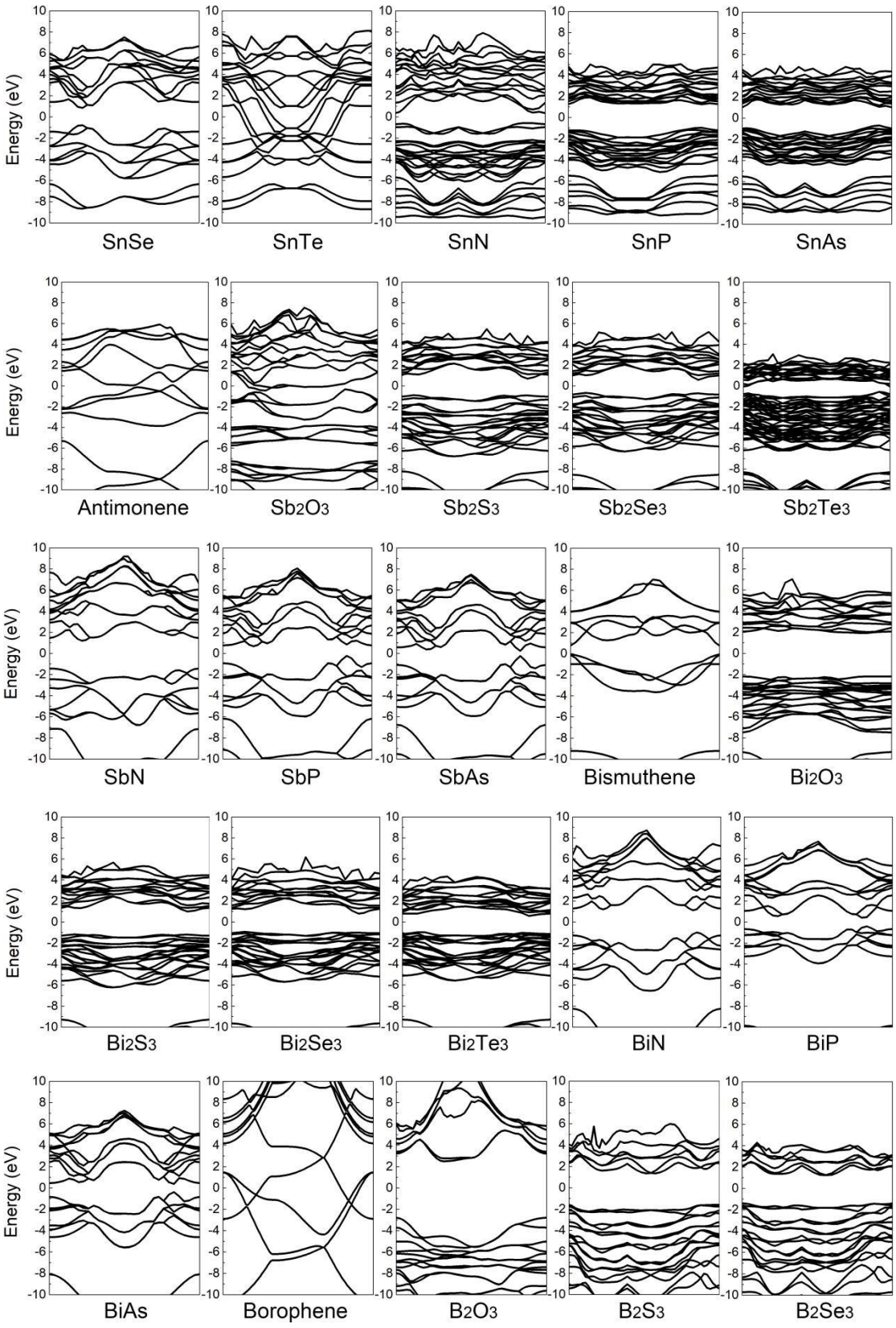
Energy (eV)
SnSe
SnTe
SnN
SnP
SnAs
Antimonene
Sb2O3
Sb2S3
Sb2Se3
Sb2Te3
SbN
SbP
SbAs
Bismuthene
Bi2O3
Bi2S3
Bi2Se3
Bi2Te3
BiN
BiP
BiAs
Borophene
B2O3
B2S3
B2Se3

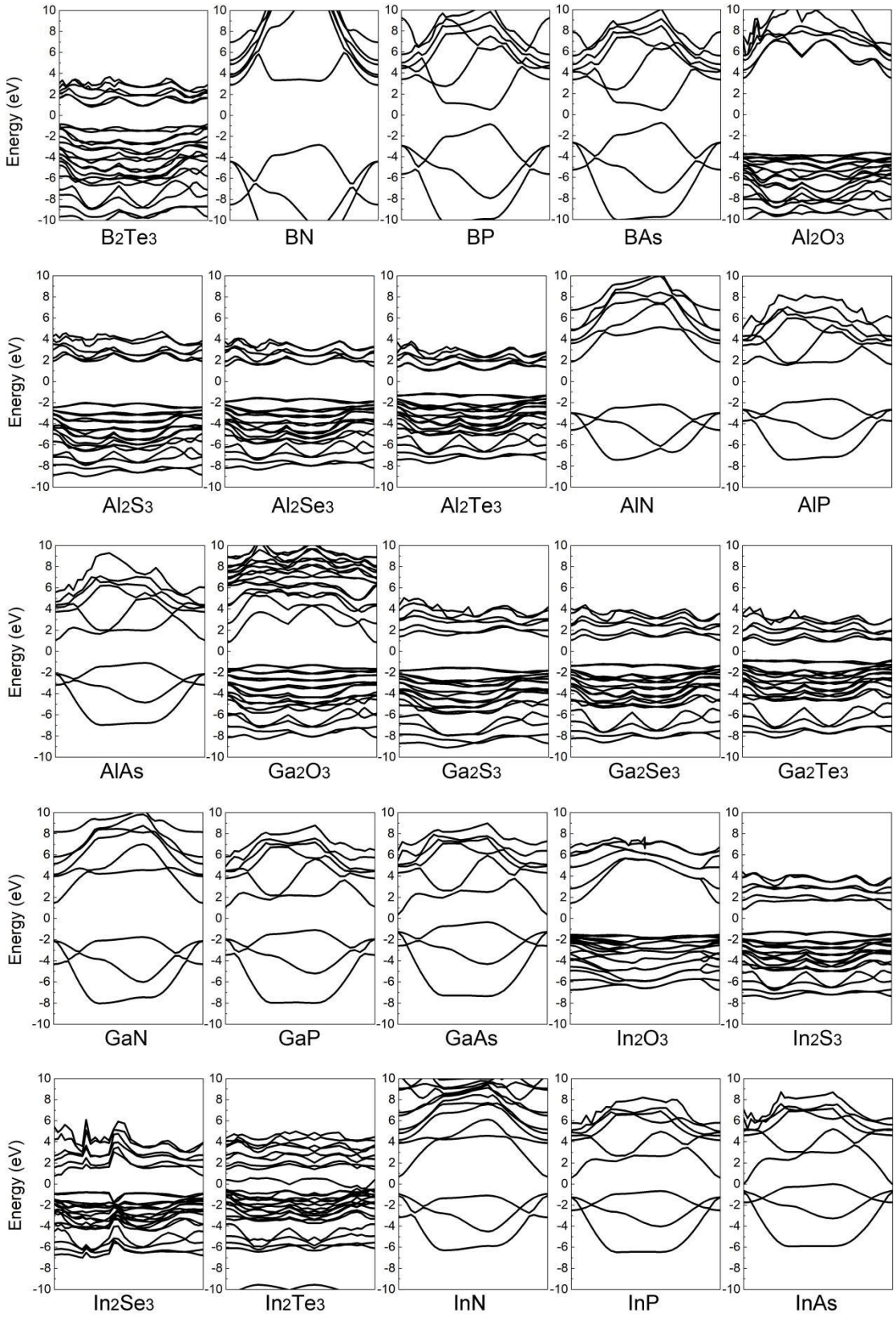
Energy (eV)
B2Te3
BN
BP
BAs
Al2O3
Al2S3
Al2Se3
Al2Te3
AlN
AlP
AlAs
Ga2O3
Ga2S3
Ga2Se3
Ga2Te3
GaN
GaP
GaAs
In2O3
In2S3
In2Se3
In2Te3
InN
InP
InAs

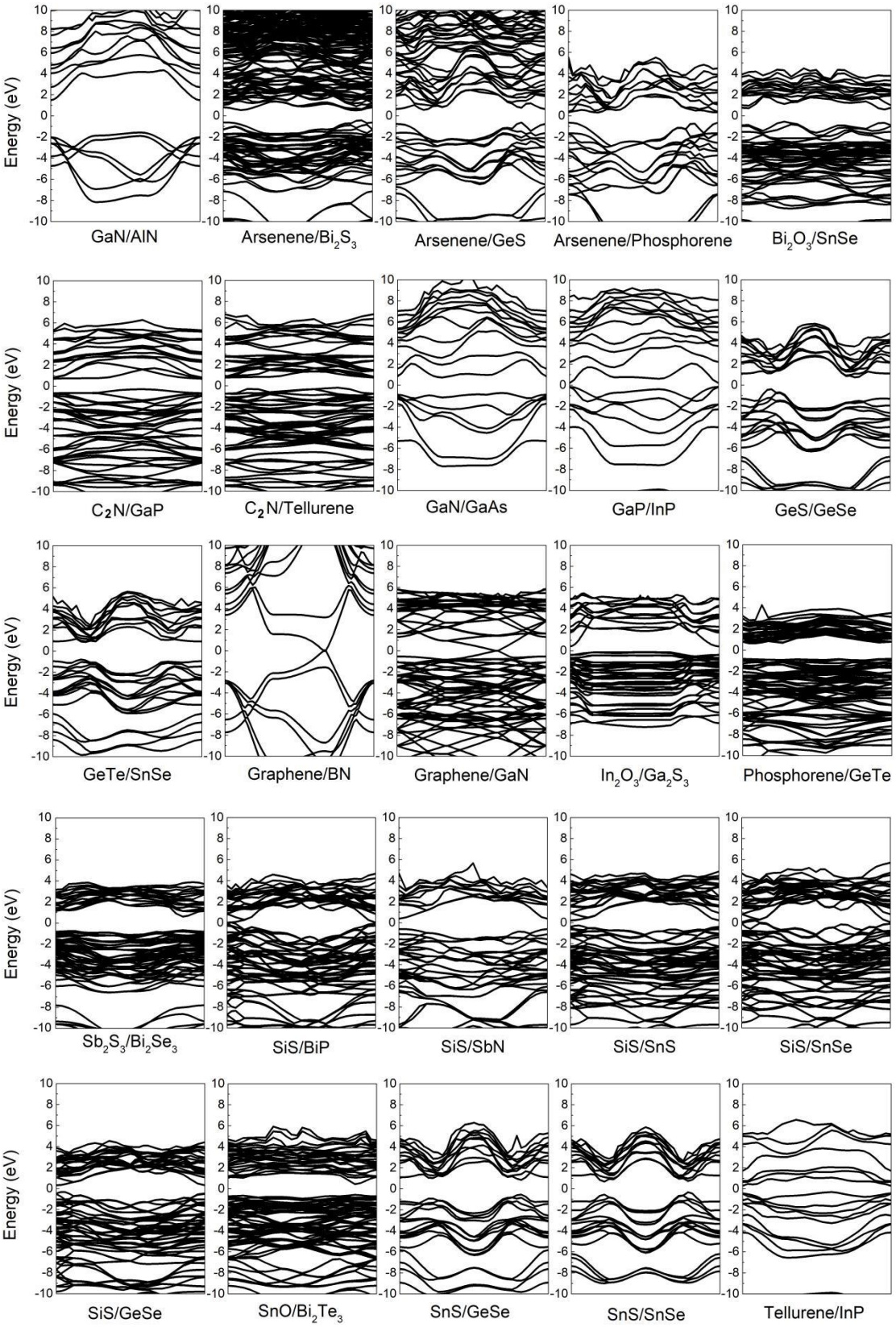

Figure S2. Band structures for 75 2D materials and 25 2D vdW heterostructures. The label of each material lies below the corresponding band structure. The Fermi level is set to zero. For an explicit comparison, the band gap center of each material is

aligned to zero.

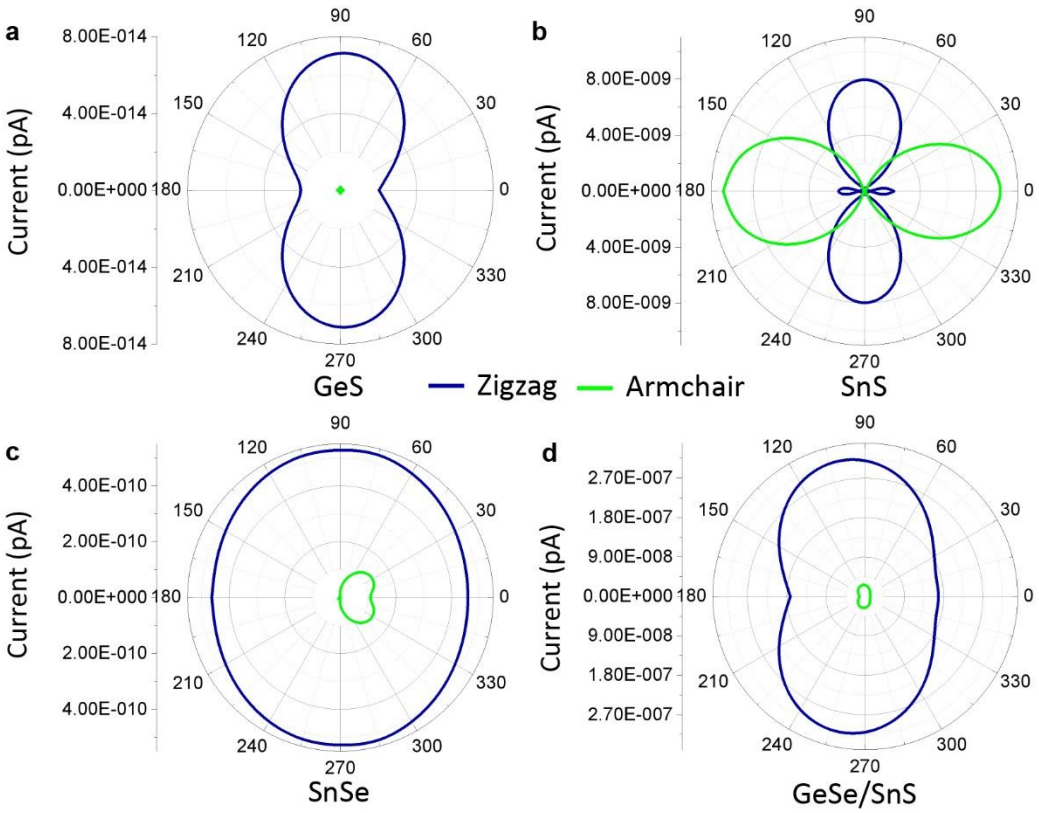

Figure S3. The calculated optoelectronic-transport properties of II-VI 2D semiconductor-based devices. (a) Polarization-sensitive photocurrents for GeS-based device are plotted with the linear-polarization laser of 638 nm in the polar coordinates. (b) Polarization-sensitive photocurrents for SnS-based device are plotted with the linear-polarization laser of 638 nm in the polar coordinates. (c) Polarization-sensitive photocurrents for SnSe-based device are plotted with the linear-polarization laser of 638 nm in the polar coordinates. (d) Polarization-sensitive photocurrents for GeSe/SnS -based device are plotted with the linear-polarization laser of 638 nm in the polar coordinates.

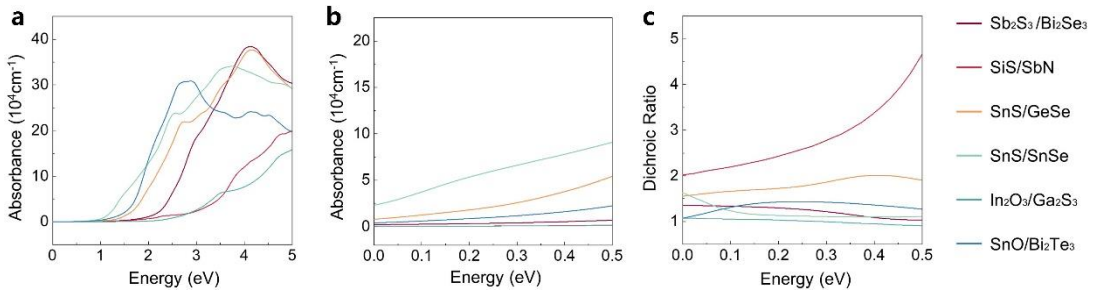

Figure S4. Optical properties of some prototypical 2D vdW heterostructures. (a) Optical absorbance of vdW heterostructures with abscissa axis starting with optical band gap. Optical absorbance (b) and dichroic ratio (c) of vdW heterostructures with abscissa axis starting with optical band gap.

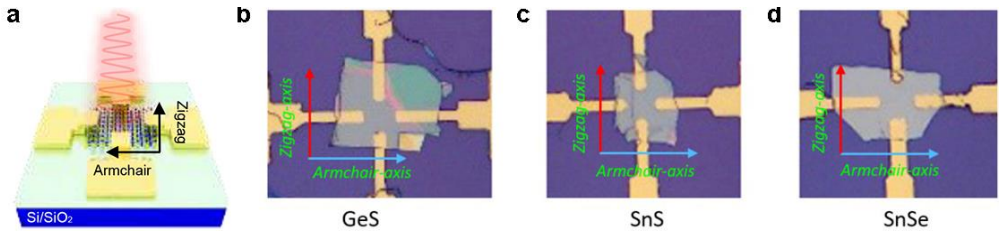

Figure S5. The schematic diagram and microscope image of the device. (a) Schematic diagram of the devices based on 2D GeS, SnS, and SnSe. (b-d) The microscope image of devices based on 2D GeS, SnS, and SnSe. Electrodes are constructed along armchair- and zigzag-*axis*, respectively.

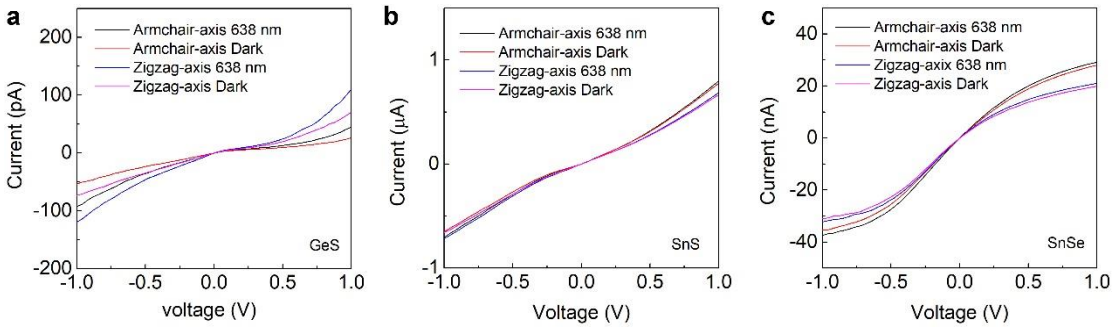

Figure S6. The output characteristics for GeS- and SnSe(S)-based photodetectors.

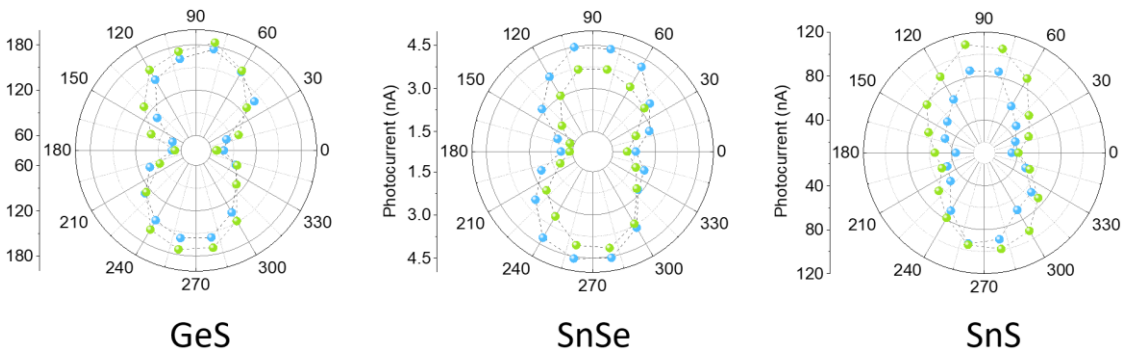

Figure S7. Experimental results of polarization-dependent photocurrent of GeS, SnSe, and SnS. (a) Polarization-sensitive photocurrents based on and GeS are plotted with the linear-polarization laser of 638 nm in the polar coordinates. (b) Polarization-sensitive photocurrents based on and SnSe are plotted with the linear-polarization laser of 638 nm in the polar coordinates. (c) Polarization-sensitive photocurrents based on and SnS are plotted with the linear-polarization laser of 638 nm in the polar coordinates.

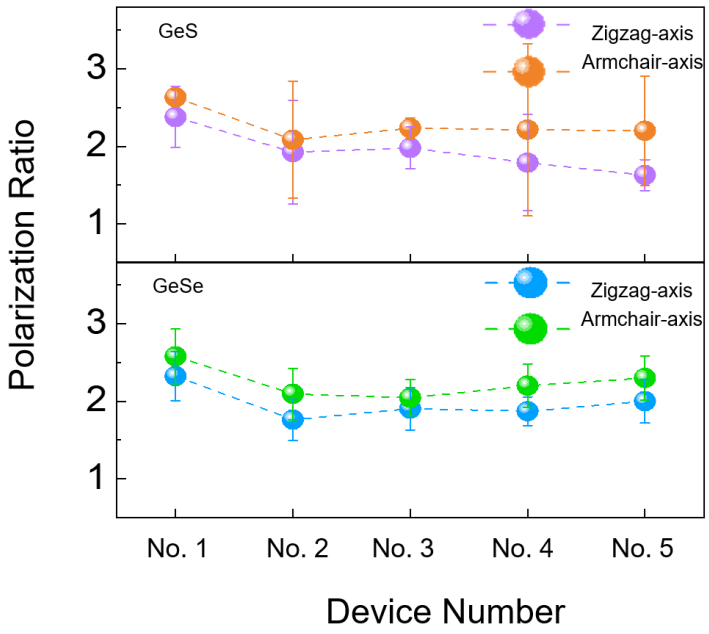

Figure S8. The polarization stability for GeSe(S)-based photodetectors. The statistical polarization ratios for these photodetectors along armchair-*axis* and zigzag-*axis* as prepared and 3 months after they were fabricated.

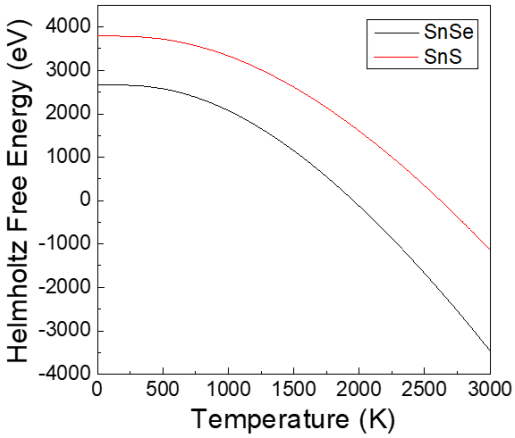

Figure S9. The stabilities for 2D SnSe and SnS. The calculated Helmholtz free energy for 2D SnSe and SnS.

Table S1. The polarization ratio values for GeSe(S)- and SbSe(S)-based devices measured as prepared and after 3 months for different devices.

		Device No.1	No.2	No.3	No.4	No.5	Mean value	Standard Deviation
As prepared	GeSe	2.1	1.57	1.88	1.7	2.1	1.878	0.23048
	GeS	1.77	2.57	2.62	2.1	1.4	2.106	0.51247
After 3 months	GeSe	2.55	1.95	2.21	2.4	2.2	2.262	0.22687
	GeS	2.67	1.54	2.17	2.3	1.49	2.034	0.50836